Chapter 19

Laser Ablation of the Microtubule Cytoskeleton: Setting Up and Working with an Ablation System

Nicola Maghelli and Iva M. Tolić-Nørrelykke

Abstract

Laser ablation is a powerful tool that can be used to study a variety of biological mechanisms. Microscopes with high optical performances are nowadays available, and lasers that could be used to perform ablations have become accessible to every laboratory. Setting up a laser ablation system is a relatively straightforward task; however, it requires some basic knowledge of optics. We illustrate the fundamental components of the experimental setup and describe the most common pitfalls and difficulties encountered when designing, setting up, and working with a laser ablation system.

Key words: Laser ablation, Optical manipulation, Microdissection, Nanosurgery

1. Introduction

Optical manipulation of living specimen has been successfully employed to investigate a variety of phenomena. Laser ablation can be used to either remove an organelle or a part of it (1, 2), or to perturb the force balance of the cellular cytoskeleton to study the mechanical equilibrium and the force generators inside a cell (3–12). In the first case, ablation allows to investigate the function of a subcellular element using an approach that is complementary to the well-established genetic tools. In the second case, the short-term modifications of the sample structure after the ablation reflect the forces acting in the sample while long-term reactions carry information about compensation or adaptation mechanisms that might be triggered by the modification.

Anne Straube (ed.), *Microtubule Dynamics: Methods and Protocols*, Methods in Molecular Biology, vol. 777,
DOI 10.1007/978-1-61779-252-6_19,

2. Materials

2.1. Optics

Custom-built two-photon setup (13), lenses, mirrors and optics holders (Thorlabs, Inc.), dichroic mirrors, filters (Chroma Technology Corp.), microscope objectives (Carl Zeiss, AG) precision mechanical hardware (OWIS GmbH).

2.2. Yeast Media (14)

1. Vitamins solution (1,000×): 1 g/l pantothenic acid (Sigma-Aldrich), 10 g/l nicotinic acid (Sigma-Aldrich), 10 g/l inositol (Sigma-Aldrich), and 10 mg/l biotin (Sigma-Aldrich).
2. Minerals solution (10,000×): 5 g/l boric acid (Sigma-Aldrich), 4 g/l manganese sulfate (Sigma-Aldrich), 4 g/l zinc sulfate hydrate ($ZnSO_4 \cdot 7H_2O$) (Sigma-Aldrich), 2 g/l iron chloride hydrate ($FeCl_2 \cdot 6H_2O$) (Sigma-Aldrich), 0.4 g/l molybdic acid (Sigma-Aldrich), 1 g/l potassium iodine (Sigma-Aldrich), 0.4 /l copper sulfate hydrate ($CuSO_4 \cdot 5H_2O$) (Sigma-Aldrich), and 10 g/l citric acid (Sigma-Aldrich).
3. Salts solution (50×): 52.5 g/l magnesium chloride hydrate ($MgCl_2 \cdot 6H_2O$) (Sigma-Aldrich), 0.735 g/l calcium chloride hydrate ($CaCl_2 \cdot 2H_2O$) (Sigma-Aldrich), 50 g/l potassium chloride (Sigma-Aldrich), and 2 g/l sodium sulfate (Sigma-Aldrich).
4. Yeast extract with supplement (YES): 5 g/l of yeast extract (Bacto), 30 g/l glucose monohydrate (Merck), 225 mg/l of Adenine, Leucine, and Uracil (Sigma-Aldrich), 150 mg/l G418 (Sigma-Aldrich), 0.67 mg/l thiamine (Sigma-Aldrich), and 1 ml/l vitamin solution.
5. Edinburgh minimal medium (EMM): 3 g/l potassium hydrogen phthalate (Sigma-Aldrich), 2.2 g/l sodium hydrogen phosphate (Sigma-Aldrich), 5 g/l ammonium chloride (Sigma-Aldrich), 20 g/l glucose monohydrate (Merck), 20 ml/l salts solution, 1 ml/l minerals solution, and 1 ml/l vitamin solution.

3. Methods

3.1. Optical Setup

To perform optical manipulations, it is necessary to visualize the structure of interest by using a microscope. Many contrast techniques, such as dark-field, DIC, or phase contrast, can be employed. However, if the sample can be labeled with fluorescent markers, then epifluorescence or confocal microscopy are of great help to clearly distinguish the feature to be ablated. In this case, the emission, excitation, and dichroic filters used to separate the excitation light from the emitted fluorescence should be taken

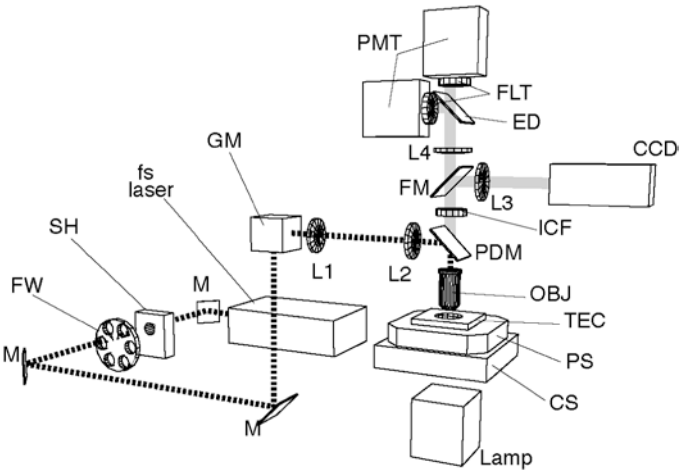

Fig. 1. Schematic of a custom-built laser ablation setup based on a near-infrared fs-pulsed laser (13). Legend: *M* mirror, *SH* shutter, *FW* filter wheel, *GM* galvanometer mirrors, *L1–L2* Keplerian telescope, *PDM* primary dichroic mirror, *OBJ* objective, *TEC* thermoelectric element, *PS* piezoelectric stage, *CS* coarse-motorized stage, *ICF* infrared cutoff filter, *FM* flip mirror, *L3–L4* collecting lenses, *ED* emission dichroic, *FLT* emission filters, *PMT* photomultiplier.

into account when designing the optical path of the ablation beam (see Note 1; Fig. 1).

3.2. Mechanical Setup

To take full advantage of the high spatial resolution that laser microdissection can achieve, the optical setup must rest on a stable and vibration-free platform. It is advisable to use a damped optical table and to avoid placing any source of mechanical noise (e.g., cooling fans, pumps, etc.) in close proximity of the ablation setup. Any high-end commercial microscope has a good intrinsic mechanical stability, whereas when developing a custom-built setup the mechanical components must also possess a good mechanical stability.

3.3. Laser Sources

Different laser sources have been successfully employed to ablate microtubules in a broad variety of organisms. The physical processes underlying the ablation process differ according to the power density of the focused light, the pulse duration, and the wavelength (15–19).

Roughly, it is possible to group the lasers into three main categories, according to their wavelength:

1. UV and near-UV lasers: The wavelength typically ranges from 325 nm emitted by an He-Cd laser (CW) to 405 nm of deep-violet laser diodes (CW or pulsed). The power ranges from 10 mW to 100 mW. Owing to the short wavelength, it is generally possible to focus the laser to a smaller area, therefore increasing the ablation accuracy compared to ablation

setups relying on visible or near-infrared laser sources (5, 6, 10, 20–22). However, when using deep-UV lasers, the optical performances of the microscope might become an issue:

- The transmission of commercially available microscope objectives starts to decrease below 400 nm, and can be as low as 50% or less for wavelength below 350 nm. Therefore, the laser power delivered to the sample that can be effectively used for ablation might be only a fraction of the total power emitted by the laser.
- The objectives are usually well-corrected against spherical and chromatic aberrations in the visible range (400–700 nm). In the UV range, the performances are worse, therefore minimizing the resolution gain given by the shorter wavelength.

Since many biologically relevant molecules have a pronounced absorption in the ultraviolet, the penetration depth of UV lasers is worse in comparison to visible or near-infrared lasers. If the structure to be ablated is deep within the sample, the ablation beam is progressively attenuated while travelling through the sample. As a consequence, it might be difficult to deliver enough power to efficiently perform ablations in thick sample using UV lasers. Under these circumstances, increasing the intensity of the ablation beam to achieve sufficient power at the ablation spot might result in a heavy collateral damage due to the sample absorption (see Notes 2 and 3). When working in vivo, it is often crucial to minimize the sample stress; therefore, UV-based setups might not be the optimal choice to ablate structures in the interior of a thick sample.

2. Visible lasers: The lasers emitting in the visible range most frequently used in ablation setups are the He–Cd laser (441 nm), the Ar–Kr ion lasers (488 and 514.5 nm), and the frequency-doubled Nd:YAG laser (532 nm). These lasers can deliver on the average more power than UV and near-UV laser sources (~100 mW to several watts). Moreover, the optical components used to deliver and focus the ablation beam on the sample have high transmissions and present low residual aberrations in the visible range. As a result, the ablation beam can be focused almost to diffraction limit (21, 23–25). The main drawback of using visible lasers for ablation is that often they emit in a range that is also employed to observe the sample. Therefore, it becomes difficult to prevent cross talks with the imaging channel. As an example, to observe eGFP-labeled samples requires a bandpass filter centered on the eGFP emission peak. Usually, the emission filters used for imaging eGFP transmit light from around 500 nm to around 550 nm. If the wavelength of the laser beam used to perform ablations falls within the transmission window of the emission

filter, and no special precautions are taken, back reflections from the optical surfaces or from the sample itself will reach the detector used for taking images, potentially damaging light-sensitive devices, such as CCDs, APD, or PMT (or in the worst case the eye of the user). These issues can be addressed by using shutters that protect the detector while the sample is exposed for ablation; however, this case requires to accurately synchronize the image acquisition with the ablation.

3. Near-infrared lasers: Recently, near-infrared-pulsed lasers have been successfully employed to perform ablations (1–4, 13, 15, 17, 26). The physical processes taking place in the sample when exposed to a short burst of highly intense light are complex, and not yet fully understood. However, multiphoton absorption, as well as optical breakdown and plasma formation might play a role (3, 15). Multiphoton absorption is achieved only at extremely high radiances (~10^{10}–10^{12} W/cm^2); to achieve such high photon densities, the laser emits short (~100 fs) pulses at high (~100 MHz) repetition rate, reaching a peak power of many kW. The most widespread femtosecond (fs)-pulsed, near-infrared laser source is the Titanium-Sapphire (Ti:Sa) laser. Its emission can be continuously tuned over a broad range of wavelengths, typically ranging from around 700 nm to around 1,000 nm. Ablation setups relying on near-infrared laser sources benefit of several advantages:
   - The scattering decreases with the inverse fourth power of the wavelength; therefore, longer wavelengths are less affected by the optical properties of the sample, and can penetrate deeper into the tissues. When performing ablations in thick samples, such as embryos, the penetration depth is a critical factor, and only near-infrared lasers are capable of efficiently ablating structures well below the sample surface.
   - Multiphoton absorption only takes places around the focal plane, and not above or below it. The energy density required for an efficient multiphoton absorption is only achieved at the focal plane, where the laser beam is focused to the smallest possible area. Above and below the focal plane, the beam diameter is larger than at the focal plane, and the energy density is not high enough to trigger multiphoton absorption. Therefore, the ablation is performed in a spatially *confined* region.
   - Many biological relevant molecules have very low absorption coefficients in the near-infrared range. Therefore, the risk of inducing unspecific damage to the sample is smaller when using near-infrared lasers than when using UV or visible lasers. Keeping the damage low is particularly

important when performing ablations of sensitive samples, and critical when working with single cells.

However, several issues must be considered when using femtosecond-pulsed, near-infrared lasers:

- Using wavelengths in the near-infrared range decreases the attainable resolution.
- The transmission and correction of microscope objectives in the near-infrared range are worse than that in the visible range, although the performance degradation is not as severe as in the case of UV and near-UV lasers.
- A femtosecond pulse undergoes distortion when travelling through materials that have a wavelength-dependent refractive index, such as the glasses commonly used for manufacturing optical components. The result is a broadening of the pulse that becomes more pronounced as the original pulse length decreases. The pulse broadening decreases the peak power and consequently lowers the multiphoton absorption efficiency (see Note 4). The net result is a less efficient ablation. For this reason, it is problematic to deliver the short pulses of the laser to the ablation setup using optical fibers. Working with free-spaced setups, and using high-power lasers might be hazardous if proper precautions concerning laser safety are not taken.
- Typically, an fs-pulsed laser is more expensive than a gas- or solid-state laser.

3.4. Positioning Control

To accurately ablate a specific target, it is necessary to precisely control the position the ablation spots on the sample. The axial position of the ablation beam with respect to the sample is usually controlled by moving the sample with respect to the objective. Simultaneous imaging while performing ablations requires the focus of the ablation beam to coincide with the focal plane of the imaging system. A relative offset, typically present when using UV or near-infrared ablation lasers as a result of chromatic aberration, can be corrected by adjusting the divergence of the ablation beam. The lateral positioning can instead be achieved either by keeping the laser beam fixed and moving the sample, or by steering the ablation beam while keeping the sample at rest with respect to the microscope. The first method is the most straightforward and simple to implement. It is usually employed when the ablation precision is not critical (see Note 5), or to ablate the sample along an extended path that would normally not fit in a single field of view of the setup. The second method is technically more complex, but offers more flexibility and permits to better control the ablation area. Usually, a couple of galvanometer scanners are employed to steer the ablation beam (see Note 6).

3.5. Coupling of the Ablation Beam

To guarantee a high spatial accuracy and coupling efficiency, the $1/e$ diameter of the ablation beam should ideally match the size of the back aperture of the microscope objective (see Note 7). The laser for ablation is typically available either as a free beam, with diameters of around 1 mm, or as output of an optical fiber. In both cases, it is necessary to insert some rely optics that will collimate and expand the beam to its correct diameter (see Notes 8 and 9). In addition, if the ablation setup implements a beam steering unit, care must be taken that the beam pivoting point is on a conjugate telecentric plane. Otherwise, scanning the beam induces a movement of the beam at the objective back aperture, changing the coupling efficiency, and therefore the total power of the laser delivered to the sample (see Note 9). As a result, the ablation efficiency depends on the position of the ablation beam in the microscope field of view. A typical solution employed to magnify and couple a collimated beam to the microscope objective is to use either a Galilean or a Keplerian telescope. The first one uses a convex and a concave lens, has a compact design, but cannot be used with a beam steering unit. The second one uses two convex lenses and can be used with a beam steering unit; however, this design needs more space.

3.6. Performing Ablations

Performing ablation in a living specimen requires a delicate balance: it is necessary to deliver enough energy to reliably disrupt the ablation target, yet the sample must not suffer too much "collateral damage." Otherwise, it becomes difficult to discriminate between the consequences of the ablation, and the artifacts due to more unspecific damage. To choose the optimal parameter set for ablation (exposure time, power, wavelength, scanned area), it is advisable to perform several test runs changing a single parameter at a time while monitoring the ablation efficiency and the insurgence of any possible unspecific damage (4, 20). The actual experiment is then performed choosing the set of parameters that maximized the ablation efficiency while still keeping the sample damage low. Once the best parameter set is found, a typical ablation experiment performed on fission yeast cells (Fig. 2) follows this protocol:

1. Grow fission yeast cells in liquid YES (50 ml) at 25°C to logarithmic phase. To ensure the homogeneity, the culture is placed on a temperature-regulated shaker.
2. Place a small aliquot (~50–100 μl) of the culture on a 35-mm glass-bottom Petri dish (Matek), which was previously coated with ~2 μl of 2 mg/ml lectin BS-1 (Sigma-Aldrich).
3. Allowed to adhere for 10 min.
4. Rinse the sample twice with 0.5 ml EMM.
5. Fill the Petri dish with 3 ml EMM with appropriate supplements for imaging.

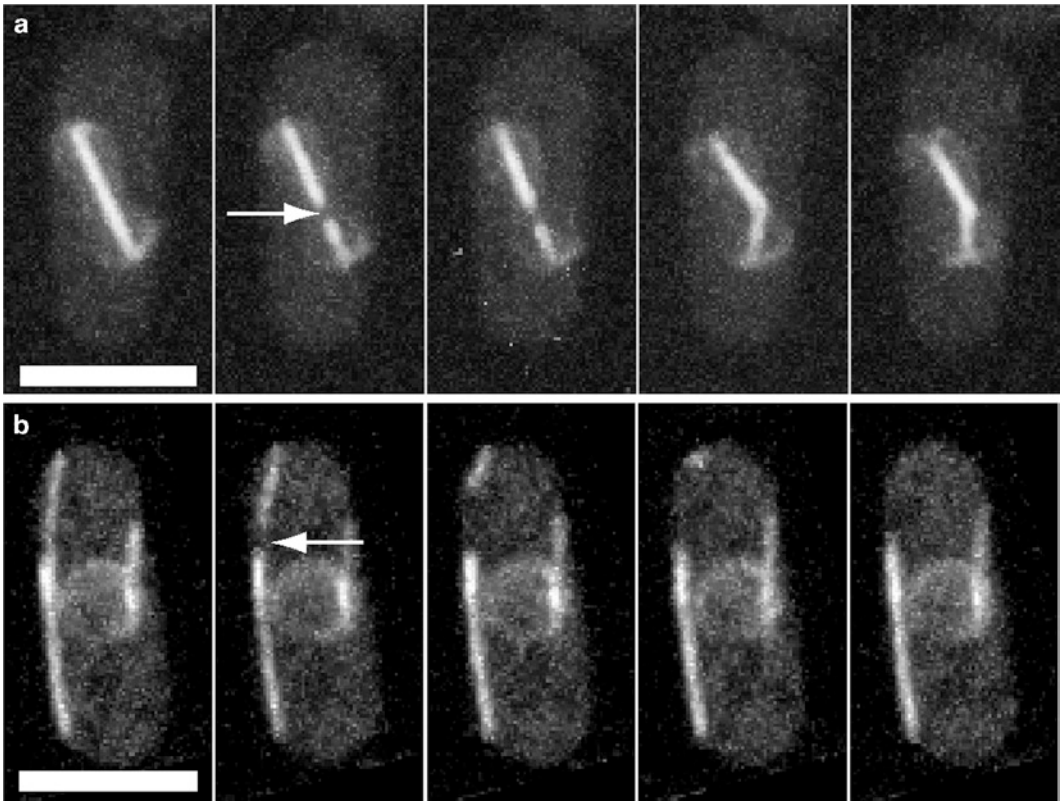

Fig. 2. Laser ablations of microtubules in *Schizosaccharomyces pombe*. The images sequences illustrate the effect of targeted irradiations (marked by the *arrows*) on microtubules. In (**a**), the mitotic spindle is destabilized. In (**b**), a microtubule is severed, and it is possible to follow the depolymerization of the detached fragment. Scale bar 5 μm, time between frames is 15 s for (**a**) and 2.5 s for (**b**). Laser ablation performed using the custom-built system described in (13). Cells expressing tubulin-GFP and cut11-GFP grown in YES medium, imaging and ablation performed in EMM medium.

6. Mount the sample on the ablation setup. Before proceeding, the thermal state of the sample is allowed to settle for approximately 10 min.
7. A suitable cell is selected. During the search, low-damage imaging (brightfield) is used.
8. Pre-ablation imaging. The sample is imaged to make sure that the structure to ablate presents no abnormalities and to provide an unperturbed reference to compare with the ablation outcome. Moreover, the user decides at this stage which region of the sample to ablate.
   In Fig. 2, pre-ablation imaging was achieved by scanning a stack of ten planes, 0.5 μm apart, at a pixel size of 100 nm/pixel using the custom-built two-photon setup described in (13). A Ti:Sa femtosecond-pulsed laser (Chameleon XR by Coherent, 150 fs nominal pulse width, 90 MHz rep. rate) tuned to 895 nm was used. The average power at the sample

plane was 3 mW. The ablation region was selected in the plane were the structure was most in focus.

9. Performing the actual ablation. During this phase the sample is exposed with the ablation beam over the area previously designated, using the optimal power and exposure time. In our case, to ablate the microtubules in Fig. 2, the average power at the sample was 100 mW while the exposure time was 50 ms for ablating the mitotic spindle (Fig. 2a) and 20 ms for interphase microtubules (Fig. 2b).
10. Post-ablation imaging. After ablating, the sample is imaged to assess the ablation outcome and to monitor the changes induced by the ablation. The same settings used for pre-ablation imaging were used.

4. Notes

1. If using polarization-sensitive components, such as Nomarski or Wollaston prisms, care must be taken to properly design the optical path of the ablation beam because the laser used for ablation might emit highly polarized light.
2. Absorption by fluorescent markers might give an important contribution to the ablation efficiency; the ablation requires less power if the wavelength is efficiently absorbed by the fluorescent marker (15, 16).
3. Depleting oxygen, by example when using oxygen scavengers to prevent fast bleaching, might decrease the ablation efficiency (15).
4. An acusto-optical modulator can provide quick control of the power of the ablation beam. However, the beam quality might be negatively influenced and, in case of a femtosecond laser, the pulses might be excessively broadened.
5. When ablating small structures, simply parking the beam over it might not be efficient. Scanning the ablation beam over a slight bigger area might give better results.
6. If the beam steering unit is mechanical (galvanometer or piezoelectric mirrors), the inertia of the moving parts may introduce residual errors in the beam positioning. To rule out these errors, it is possible to record the beam position at various positioning speed and compensate the steering system consequently.
7. Slightly overfilling the objective with the ablation beam (i.e., magnifying the ablation beam to a diameter larger than the diameter of the back aperture of the microscope objective)

might help compensating for any residual misalignment introduced by a beam steering system.

8. To facilitate the coupling of the ablation beam, it is possible to start using a low magnification objective (5× or 10×) to check the coarse alignment and then switch to higher magnifications for the fine adjustments.
9. Aligning a near-infrared laser might be troublesome. If using a Ti:Sa laser, it is sometimes possible to tune the laser to a visible wavelength, perform the alignment, and then switch back to near-infrared for ablation. Alternatively, a visible laser might be aligned to the infrared beam and then used as a reference.
10. If a steering unit controls the ablation beam, it is critical to calibrate the beam position with respect to the imaging field of view. A quick method consists in bleaching spots over a uniformly fluorescent polymer.

References

1. Stiess, M., Maghelli, N., Kapitein, L. C., Gomis-Ruth, S., Wilsch-Brauninger, M., Hoogenraad, C. C., Tolic-Norrelykke, I. M., and Bradke, F. (2010) Axon extension occurs independently of centrosomal microtubule nucleation, *Science 327*, 704–707.
2. Sacconi, L., O'Connor, R. P., Jasaitis, A., Masi, A., Buffelli, M., and Pavone, F. S. (2007) In vivo multiphoton nanosurgery on cortical neurons, *J Biomed Opt 12*.
3. Vogel, S. K., Pavin, N., Maghelli, N., Julicher, F., and Tolic-Norrelykke, I. M. (2009) Self-organization of dynein motors generates meiotic nuclear oscillations, *PLoS Biol 7*, e1000087.
4. Sacconi, L., Tolic-Norrelykke, I. M., Antolini, R., and Pavone, F. S. (2005) Combined intracellular three-dimensional imaging and selective nanosurgery by a nonlinear microscope, *J Biomed Opt 10*, 14002.
5. Colombelli, J., Reynaud, E. G., and Stelzer, E. H. (2005) Subcellular nanosurgery with a pulsed subnanosecond UV-A laser, *Med Laser Appl 20*, 217–222.
6. Colombelli, J., Reynaud, E. G., Rietdorf, J., Pepperkok, R., and Stelzer, E. H. (2005) In vivo Selective Cytoskeleton Dynamics Quantification in Interphase Cells Induced by Pulsed Ultraviolet Laser Nanosurgery, *Traffic 6*, 1093–1102.
7. Tolic-Norrelykke, I. M., Sacconi, L., Thon, G., and Pavone, F. S. (2004) Positioning and elongation of the fission yeast spindle by microtubule-based pushing, *Curr Biol 14*, 1181–1186.
8. Khodjakov, A., La Terra, S., and Chang, F. (2004) Laser microsurgery in fission yeast; role of the mitotic spindle midzone in anaphase B, *Curr Biol 14*, 1330–1340.
9. Botvinick, E. L., Venugopalan, V., Shah, J. V., Liang, L. H., and Berns, M. W. (2004) Controlled ablation of microtubules using a picosecond laser, *Biophys J 87*, 4203–4212.
10. Spurck, T., Stonington, O., Snyder, J., Pickett-Heaps, J., Bajer, A., and Mole-Bajer, J. (1990) UV microbeam irradiations of the mitotic spindle. II. Spindle fiber dynamics and force production, *J Cell Biol 111*, 1505.
11. Grill, S. W., Howard, J., Schaffer, E., Stelzer, E. H., and Hyman, A. A. (2003) The distribution of active force generators controls mitotic spindle position, *Science 301*, 518–521.
12. Tolic-Norrelykke, I. M. (2008) Push-me-pull-you: how microtubules organize the cell interior, *Eur Biophys J 37*, 1271–1278.
13. Maghelli, N., and Tolic-Norrelykke, I. M. (2008) Versatile laser-based cell manipulator, *J Biophotonics 1*, 299–309.
14. Moreno, S., Klar, A., and Nurse, P. (1991) Molecular genetic analysis of fission yeast Schizosaccharomyces pombe, *Methods Enzymol 194*, 795–823.
15. Vogel, A., Noack, J., Hüttman, G., and Paltauf, G. (2005) Mechanisms of femtosecond laser nanosurgery of cells and tissues, *Appl Phys B 81*, 1015–1047.

16. Vogel, A., and Venugopalan, V. (2003) Mechanisms of pulsed laser ablation of biological tissues., *Chem Rev 103*, 577–644.
17. König, K., Riemann, I., Fischer, P., and Halbhuber, K. J. (1999) Intracellular nanosurgery with near infrared femtosecond laser pulses, *Cellular and molecular biology (Noisy-le-Grand, France) 45*, 195–201.
18. Berns, M. W., Wright, W., and Wiegand Steubing, R. (1991) Laser microbeam as a tool in cell biology, *Int Rev Cytol 129*, 1–44.
19. Heisterkamp, A., Maxwell, I. Z., Mazur, E., Underwood, J. M., Nickerson, J. A., Kumar, S., and Ingber, D. E. (2005) Pulse energy dependence of subcellular dissection by femtosecond laser pulses, *Opt Express 13*, 3690–3696.
20. Raabe, I., Vogel, S. K., Peychl, J., and Tolic-Norrelykke, I. M. (2009) Intracellular nanosurgery and cell enucleation using a picosecond laser, *J Microsc 234*, 1–8.
21. Aist, J. R., Liang, L. H., and Berns, M. W. (1993) Astral and spindle forces in PtK2 cells during anaphase B: a laser microbeam study, *J Cell Sci 104*, 1207–1216.
22. Leslie, R., and Pickett-Heaps, J. (1983) Ultraviolet microbeam irradiations of mitotic diatoms: investigation of spindle elongation, *J Cell Biol 96*, 548–561.
23. Moore, J. K., Magidson, V., Khodjakov, A., and Cooper, J. A. (2009) The spindle position checkpoint requires positional feedback from cytoplasmic microtubules, *Curr Biol 19*, 2026–2030.
24. Aist, J. R., and Berns, M. W. (1981) Mechanics of chromosome separation during mitosis in Fusarium (Fungi imperfecti): new evidence from ultrastructural and laser microbeam experiments., *J Cell Biol 91*, 446–458.
25. Berns, M. W., Rattner, J., Brenner, S., and Meredith, S. (1977) The role of the centriolar region in animal cell mitosis. A laser microbeam study, *J Cell Biol 72*, 351–367.
26. König, K., Liang, L. H., Berns, M. W., and Tromberg, B. J. (1995) Cell damage by near-IR microbeams, *Nature 377*, 20–21.